Supporting Information

Biphasic Electron Transfer Arising from Two Non-Interacting Donating States Unambiguously Revealed in C343 Sensitized Mesoporous SnO_2 by Combining Two Complementary Time-Resolved Spectroscopy Techniques

Miguel Ángel Pulido-Lendínez[1], Marco Ballabio[1], Andrés Burgos-Caminal[1,2], María E. Corrales[2,3], Sergio Revuelta[1], Saül Garcia-Orrit[1], Víctor Vega-Mayoral[1], Juan Cabanillas-González[1], Luis Bañares[1,4], Wojciech Gawelda[1,2], and Enrique Cánovas[1]*

[1] *Instituto Madrileño de Estudios Avanzados en Nanociencia (IMDEA Nanociencia), Calle Faraday 9, 28049 Madrid, Spain.*

[2] *Departamento de Química, Facultad de Ciencias, Universidad Autónoma de Madrid, Calle Francisco Tomás y Valiente 7, 28049 Madrid, Spain.*

[3] *Departamento de Química Física Aplicada, Facultad de Ciencias, Universidad Autónoma de Madrid, Calle Francisco Tomás y Valiente 9, 28049 Madrid, Spain*

[4] *Departamento de Química Física and Center for Ultrafast Lasers (CLUR), Facultad de Ciencias Químicas, Universidad Complutense de Madrid, Plaza de las Ciencias 2, 28040 Madrid, Spain.*

[5] *Center for Ultrafast Lasers (CLUR), Facultad de Ciencias Químicas, Universidad Complutense de Madrid, Plaza de las Ciencias 2, 28040 Madrid, Spain.*

* *E-mail:* enrique.canovas@imdea.org

S1. C343-SnO_2 sample preparation

Figure S1 illustrates the step-by-step procedure to fabricate the C343-SnO_2 film after the preparation of SnO_2 paste via the sonication method described previously.[1] First, we mix 1g of SnO_2 powder (≤ 100nm avg. part. size, 549657-25G, Sigma Aldrich) in 10mL of ethanol (EtOH) (Purity (GC) ≥ 99.9% for spectroscopy Uvasol®, 1.00980.0500, Supelco) and separately 4g of terpineol (mixture of isomers ≥ 96%, W304506-1KG-K, Sigma Aldrich) in 8mL EtOH, followed by the addition of 0.5g of ethyl cellulose (48.0-49.5% (w/w) ethoxyl basis, 46070-250G-F, Sigma Aldrich). The terpineol-ethyl cellulose mixture is then added to SnO_2 in EtOH dispersion. After 3 cycles of 5 min sonication and 1 min rest, we evaporate the EtOH in a fumehood for 2 hours, until we reach a thick slurry.

Once we dip coat the SnO_2 paste onto a fused silica substrate by doctor blade (tape casting),[2-3] we sinter the SnO_2 layer through a two steps heating process[2] on a hotplate (PR 5-3T PID Programme Regulator, Harry Gestigkeit): 1) From room temperature to 150ºC in 20min, maintained for 1h, 2) from 150ºC to 400ºC in 1h, maintained for 2h. This procedure leads changes in SnO_2 bandgap which should not compromise ET to take place once the dye-MO is excited, i.e., SnO_2 bandgap increase is expected to be less than 0.64 eV when annealing at 400ºC.[4]

For the C343 in solution, we use a 0.3mM concentration of C343 dye (≥ 97%, 393029-100MG, Sigma Aldrich) diluted in a 1:1 acetonitrile:ethanol mixture,[5] (1:1 ACN&EtOH, ACN: Assay (GC) ≥ 99.5% Spectronorm for spectroscopy, BDH1103-4LP, VWR Chemicals BDH)). To obtain the dye-MO film, the SnO_2 films are heated again from room temperature to 150ºC in 20 min, and then we submerge the SnO_2 film in the C343 solution for about 20 hours. The resulting C343-SnO_2 film is rinsed with EtOH to remove the excess dye and is left to dry in a fume hood.

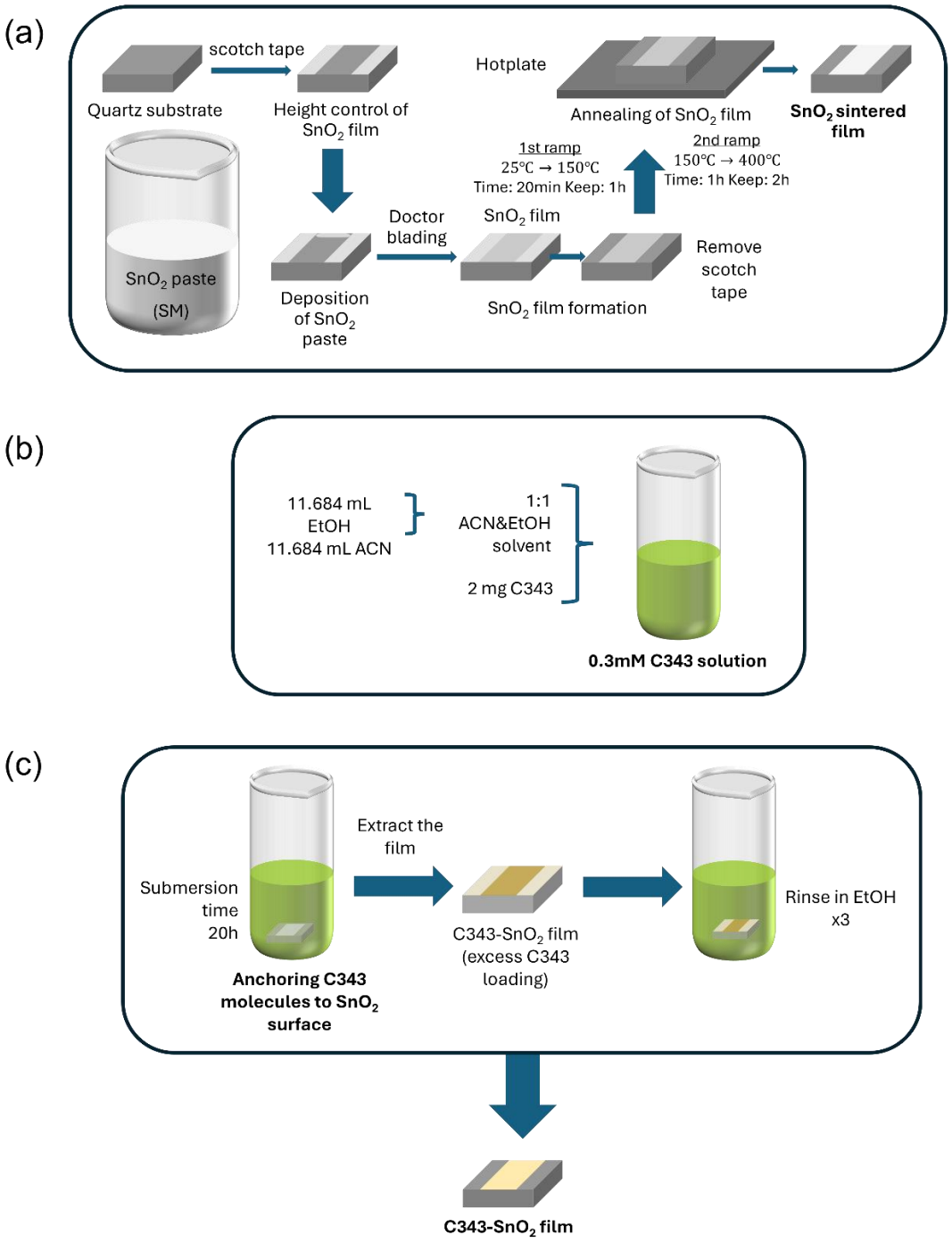

Figure S1. Scheme for the fabrication of a C343-SnO_2 film. (a) Fabrication of the SnO_2 sintered film. (b) Preparation of a 0.3 mM C343 in a 1:1 EtOH&ACN solution. (c) Sensitization of the C343-SnO_2 film.

S2. Profilometer and atomic force microscopy (AFM) measurements on a C343-SnO_2 film

We employed a profilometer to characterize the C343-SnO_2 thickness (Figure S2a-b), which yielded a thickness of 10-15 μm. Additionally, by AFM measurements we have characterized the surface roughness of a C343-SnO_2 film, as well as from a SnO_2 film, in three different 15x15 μm^2 areas. AFM measurements were carried out in a commercial AFM system (JPK Nanowizard 2, Bruker) in intermittent contact (dynamic) mode using scanning by probe configuration in ambient conditions. Rectangular silicon cantilevers HQ:XSC11-D (Mikromash) were used with a tip radius of 8 nm. Their nominal spring constant is 42 N/m and its resonance frequency is ~350 kHz. All the AFM images have been processed with JPK Data Processing software using the leveling (flattening) tool.

Regarding the C343-SnO_2 film, for area 1 (not shown), the surface roughness is 204.8 nm; in area 2 (not shown), the roughness is 142.7 nm; for area 3 (Figure S2c), the roughness is 127.5 nm. In the case of the SnO_2 alone (Figure S2d), the surface roughness of area 1, 2 and 3 are 414.6 nm, 209.3 nm, and 163.3 nm. Figure S2d shows only the latter area.

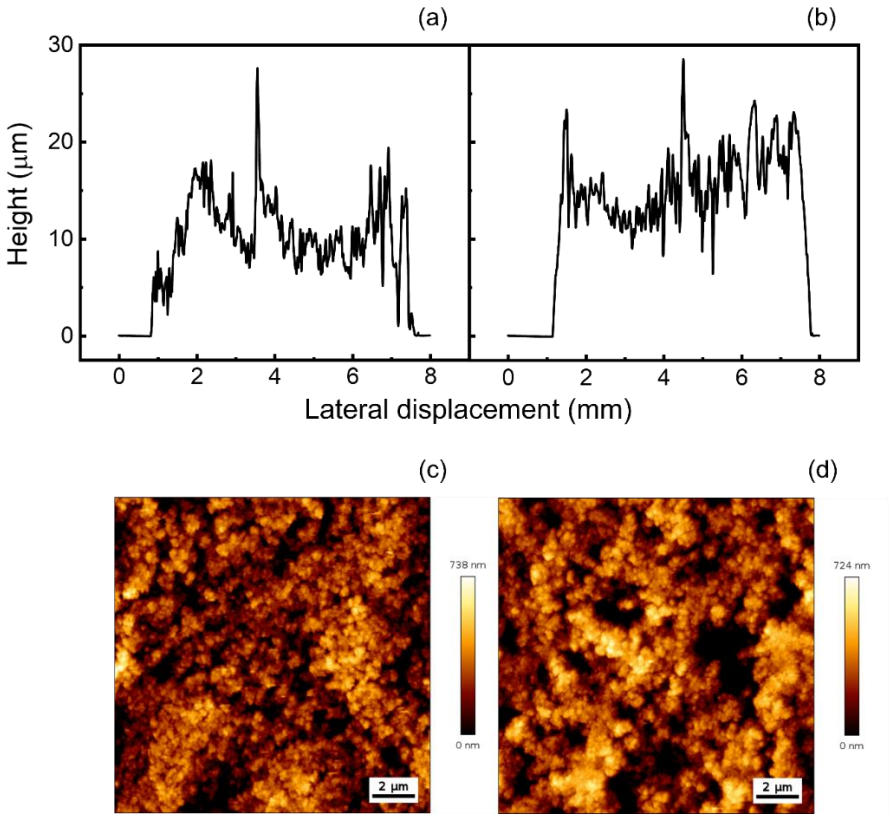

Figure S2. Topographic characterization of fabricated films. (a-b) Profilometer measurements of two C343-SnO_2 films. (c) AFM images of a 15x15 μm^2 area of the C343-SnO_2 film measured in (a). (d) AFM images of a 15x15 μm^2 area of a SnO_2 film.

S3. C343 and SnO_2 energy levels alignment

The C343 HOMO-LUMO bandgap has been assigned in literature with a value of 2.291 eV for free molecules, which reduces to 2.196 eV when C343 molecules are adsorbed onto a TiO_2 cluster.[6] The LUMO and HOMO levels of C343 when adsorbed have reported values of 1.033 eV and -1.163 eV,[6] where both levels have been shifted to set the zero energy to the lower edge of the semiconductor CB.[6] The bandgap of the bulk SnO_2 is reported to be ranging from 3.60 to 3.99 eV.[7-9]

S4. Pump diameter in FLUPS transmission and reflection measurements

To characterize ET in the C343-SnO_2 film by FLUPS[10] we excite the dye, first in a solvent solution (which acts as a reference) and then in the dye-MO film. Fluorescence emission (FL) is collected in transmission for the dye in a solvent solution (pump diameter, 49 μm). Since the dye is diluted inside a 2 mm thick cuvette, measurement in reflection results in the emission coming out of a slanted line, which is complicated to collect with parabolic mirrors. However, measuring the dye solution in transmission ensures that everything is in the same horizontal and vertical position and is better collected and focused. Nevertheless, because of the opacity of the dye-MO film, measurements in transmission are not viable. Therefore, in this latter case we perform FLUPS in reflection mode (pump diameter, 150 μm). Furthermore, this geometry prevents the pump from passing through unnecessary substrate volume and signal interferences between the dye-MO and the substrate, thus avoiding reflections from the substrate. Another advantage of the thin dye-MO films is that all the FL comes out of a small volume, which allows us to better focus the FL onto the 0.1 mm slab BBO crystal for up-conversion. Since the spot diameters for C343 and C343-SnO_2 are different, due to the geometries we have used to measure the FL, we have changed the energy of the pump pulse between both type of measurements for the pump fluence to be the same.

S5. Pump fluence dependence measurements in FLUPS

We have performed FLUPS measurements at different pump fluences for C343 in solution (Figure S3a-c), and for C343-SnO_2 film (Figure S3d-f). The linear behavior indicates that, for both C343 in solution (Figure S3g) and C343-SnO_2 film (Figure S3h), we measure the same dynamics regardless of the fluence and the integrated emission region.

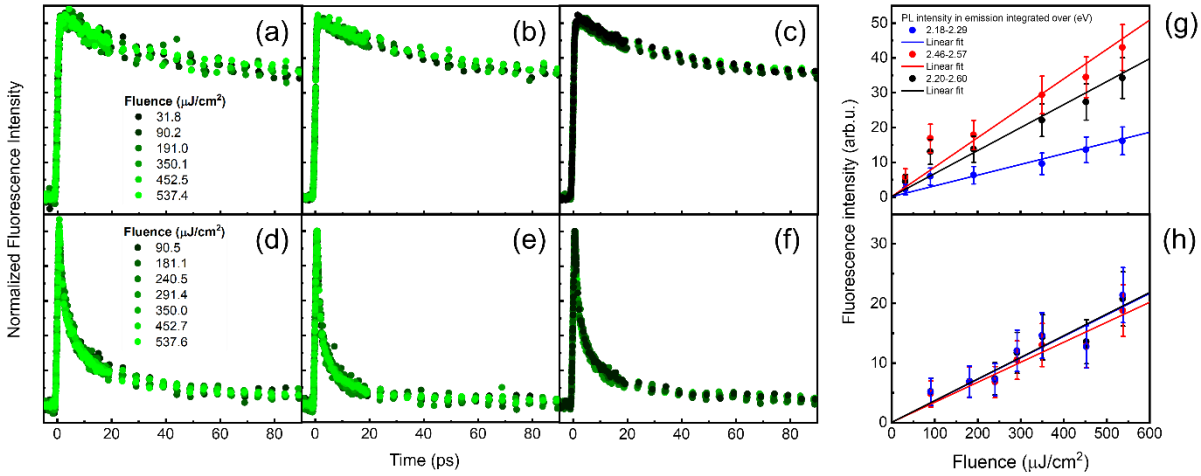

Figure S3. (a) Normalized temporal traces of FL intensity for six pump fluences at C343 in solution for the emission integrated over 2.18-2.29 eV. (b) Same for 2.46-2.57 eV. (c) Same for 2.20-2.60 eV. (d) Normalized intensity of FL for seven pump fluences at C343-SnO_2 film for the emission integrated over 2.18-2.29 eV. (e) Same for 2.46-2.57 eV. (f) Same for 2.20-2.60 eV. (g) Intensity of FL at the peak of maximum emission (i.e., right after photoexcitation) as a function of pump fluence at C343 in solution. Blue, red, and black dashed lines are linear fits for the three probe energy regions. (h) Intensity of FL at the peak of maximum emission as a function of pump fluence at C343-SnO_2 film. Blue, red and black lines are linear fits for the three probe energy regions.

In first approximation, from the biphasic exponential decay for the temporal trace of the C343-SnO_2 interface, in the emission integrated over 2.46-2.57 eV, we obtain lifetimes of $\tau_{1,C343\text{-}SnO_2}$ = 1.1 ± 0.1 ps (79 ± 2 %) and $\tau_{2,C343\text{-}SnO_2}$ = 15 ± 2 ps (21 ± 2 %) (see S10). For the FL integrated over 2.18-2.29 eV, the biexponential fits gives lifetimes of $\tau_{1,C343\text{-}SnO_2}$ = 1.9 ± 0.2 ps (65 ± 3 %) and $\tau_{2,C343\text{-}SnO_2}$ = (22 ± 2) ps (35 ± 3 %) (see S10). Both lifetimes and their relative amplitudes differ from those in the FL integrated over 2.46-2.57 eV, which suggest that there are two independent species of C343 injecting carriers to the SnO_2. This scenario is also suggested in the main text (Figure 1d). There, the FL integrated over 2.2-2.6 eV persists 5ps after photoexcitation, which also happens in the FL integrated over the 2.18-2.29 eV region, whereas the FL integrated over the 2.46-2.57 eV region has vanished at that time. We show stronger confirmation about independent ET channels in the main text by two global fits (see Figure 3).

S6. Time-Resolved Photoluminescence (TRPL) measurement of C343 in solution

To corroborate the FL lifetime from the C343 in solution obtained through FLUPS, we have performed TCSPC measurements (HydraHarp, PicoQuant). Figure S4a depicts the FL of the C343 in solution (black dots) and its respective fitting curve (red line), a single exponential decay convoluted with a Gaussian function (~260 ps). The residuals of the fitting curve are shown in Figure S4b. A fair approximation is to assign the single decay to a FL process within the dye.[11-12] We can thus express the decay lifetime in C343

as $\tau_{C343} = 1/k_{FL}$. In that sense, we have obtained a lifetime of $\tau_{C343} = (3.86 \pm 0.01)$ ns, a value in accordance with previous reports.[13-15]

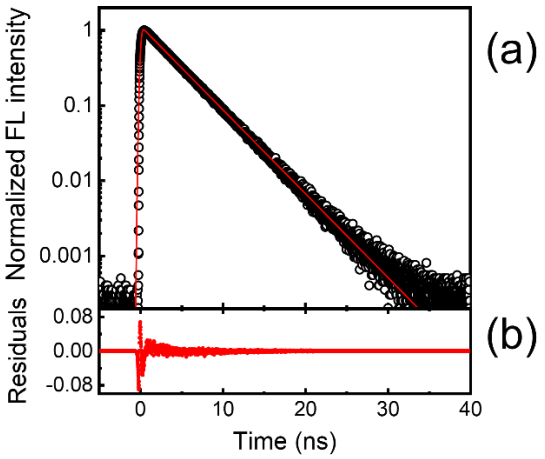

Figure S4. (a) Normalized temporal trace of FL intensity (log scale) from C343 in a 0.01 mM EtOH solution (black dots) for a time window of 30 ns with fitting curve (red solid line). (b) Residuals of the fitting curve.

S7. Fast lifetime in FLUPS measurement of C343 in solution

To determine the nature of the fast lifetime in the C343 solution in the fitting of FLUPS data, which we claim to be an artifact of the FLUPS setup rather than coming from a physical process, we have measured away from magic angle condition (Figure S5a), which yields a similar fast lifetime component. Furthermore, we have observed that this fast lifetime does not arise when using high fluence (Figure S5b) or from using ACN instead of EtOH as a solvent (Figure S5c). In this last situation, we show that the change in solvent only affects the long-lifetime value. The lifetimes and relative amplitudes for the data fitted in Figure S5 are summarized in Table S1.

We have checked that the short lifetime in Figure S3 arises as an artifact, imputed to scattered light and/or anisotropy in previous study,[16] although for the C343 in solution the FLUPS measurements have been done in a magic angle configuration (Figure S5a). Relaxation processes, such as solvent reorganization, should be followed by a spectral redshift of the FL,[17-19] which we do not observe (Figure S6). Consequently, we can consider that the only contribution from a FL decay process is given by the long lifetime.

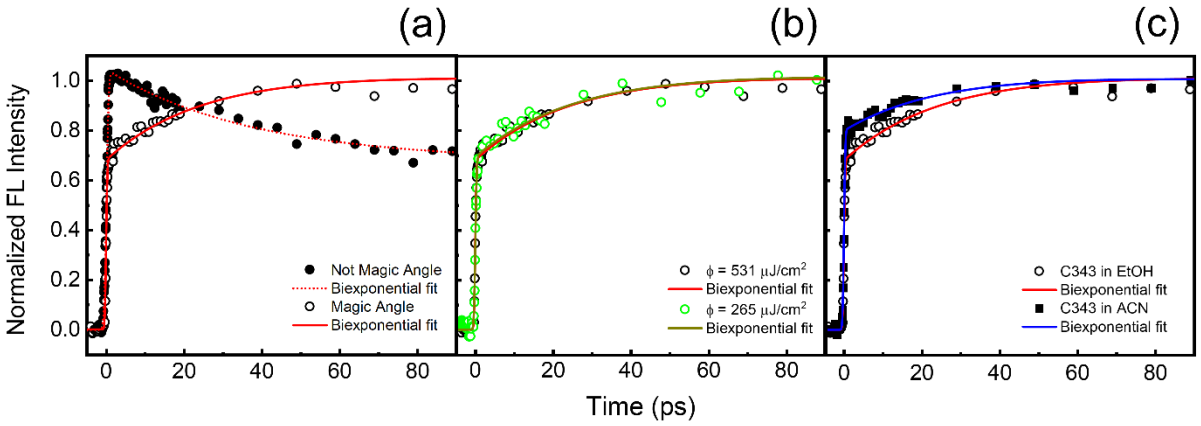

Figure S5. Normalized temporal trace of the FL intensity from C343 in a 0.3 mM solution under different conditions. (a) In a 0.3 mM EtOH solution, under magic angle condition at a pump fluence of 531 μJ/cm^2 (black empty dots), and away from magic angle condition at a pump fluence of 191 μJ/cm^2 (black solid dots). Fitting curves are indicated in red by straight line for magic angle condition and with a short dots line for the measurement away from magic angle condition. (b) In a 0.3mM EtOH solution at two pump fluences: 531 μJ/cm^2 (black empty dots) and 265 μJ/cm^2 (green empty dots). Fitting curves are indicated by red straight line for 531 μJ/cm^2 and by dark yellow line for 265 μJ/cm^2. (c) In a 0.3mM solution of EtOH (black empty dots) and in a 0.3 mM solution of acetonitrile, ACN (black solid squares). Fitting curves are indicated by red straight line for C343 in the EtOH solution, and by blue straight line for C343 in the ACN solution.

Figure		Short lifetime (ps)	Relative amplitude (%)	Long lifetime (ps)	Relative amplitude (%)
S3a	Magic Angle	25 ± 2	26 ± 1	4100 ± 100	74 ± 1
	Not Magic Angle	36 ± 3	33 ± 1	4200 ± 200	67 ± 1
S3b	High fluence	25 ± 2	26 ± 1	4100 ± 100	74 ± 1
	Low fluence	26 ± 3	25 ± 1	3900 ± 100	75 ± 1
S3c	In EtOH	25 ± 2	26 ± 1	4100 ± 100	74 ± 1
	In ACN	24 ± 2	19 ± 1	3590 ± 70	81 ± 1

Table S1. Lifetimes and relative amplitudes of the fitting curves plotted in Figure S5.

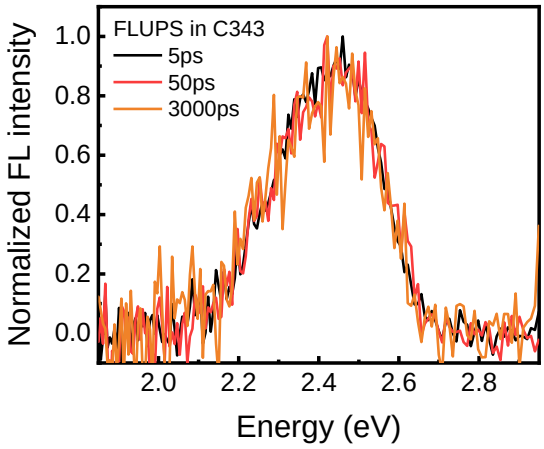

Figure S6. Normalized temporal trace of the FL intensity from C343 in a 0.3 mM EtOH solution under different times (in ps).

S8. Dynamic model in presence of two ET channels

The dynamic model of two ET channels that we propose to analyze FLUPS and TRTS data, considers the following scenario:

1) C343 in solution: Electrons relax from LUMO to HOMO mainly via photon emission with a rate $k_{FL} = k_{rad} + k_{nrad}$. Here we have essentially a two-level rate equation:

$$\frac{dN_{LUMO}(t)}{dt} = -k_{FL}N_{LUMO}(t) \qquad \text{(Eq. S1)}$$

Whose analytical solution is

$$N_{LUMO}(t) = N_{LUMO,0}\exp\left(-\frac{t}{\tau_{C343}}\right) \qquad \text{(Eq. S2)}$$

where the FL lifetime is the lifetime of the C343 in solution:

$$\tau_{C343} = \frac{1}{k_{FL}} \qquad \text{(Eq. S3)}$$

Since in FLUPS data for C343 in solution we suppose the presence of an artifact, whose rate we label as $k_{artf} \equiv 1/\tau_{artf}$, we use a double exponential fitting curve to explain the trace:

$$N_{LUMO}(t) = A_{artf}\exp\left(-\frac{t}{\tau_{artf}}\right) + N_{LUMO,0}\exp\left(-\frac{t}{\tau_{C343}}\right) \qquad \text{(Eq. S4)}$$

2) C343-SnO_2 interface: Electrons arrive to the CB of SnO_2 from two independent LUMO levels. We assume a four-level system, structured in the following way: two independent LUMO levels for each of the two types of configurations of C343 molecules onto the SnO_2 surface, one level for the CB of the SnO_2 and one, effective ground state We label their populations as $N_{LUMO,1}$ (t) and $N_{LUMO,2}$ (t), N_{CB} (t) and N_{eff} (t), respectively. Right after photoexcitation (t = 0), we impose that only the C343 LUMO levels

are populated. These fix the initial boundary conditions to $N_{LUMO,1}$ (0) = $N_{LUMO1,0}$, $N_{LUMO,2}$ (0) = $N_{LUMO2,0}$, $N_{CB,0}$ (0) = 0, and $N_{eff,0}$ (0) = 0. These populations communicate only through two channels:

- Electron Transfer: Both LUMO populations, $N_{LUMO,1}$ (*t*) and $N_{LUMO,2}$ (*t*), which independently inject electron to the SnO_2 CB. We label the rates of both injections as k_{ET1} for $N_{LUMO,1}$ (*t*) and k_{ET2} for $N_{LUMO,2}$ (*t*).
- Effective recombination: Electrons leave the SnO_2 CB via multiple channels (*i.e.* back electron transfer from CB to the HOMO of each C343 molecule). We label the rate of the effective channel as k_{eff}.

For the interface we ascribe each component of the temporal trace to a competition between an independent ET and FL channels. Therefore, we can write each of the two lifetimes for the temporal trace of FL in the C343-SnO_2 interface as:

$$\tau_{\mathrm{C343-SnO_2},i} = \frac{1}{k_{ET,i}+k_{FL}} \quad \text{(Eq. S5)}$$

where i = 1,2. For the C343-SnO_2 interface we have also assumed that the sensitization of SnO_2 by C343 molecules does not introduce additional radiative pathways ($k_{FL}^{\mathrm{C343\text{-}SnO_2}} \approx k_{FL}^{\mathrm{C343}}$). Then, the dynamic model of two ET channels for the C343-SnO_2 interface is described by the following system of differential equations:

$$\frac{dN_{LUMO_1}(t)}{dt} = -k_{ET_1}N_{LUMO_1}(t) \quad \text{(Eq. S6)}$$

$$\frac{dN_{LUMO_2}(t)}{dt} = -k_{ET_2}N_{LUMO_2}(t) \quad \text{(Eq. S7)}$$

$$\frac{dN_{CB}(t)}{dt} = k_{ET_1}N_{LUMO_1}(t) + k_{ET_2}N_{LUMO_2}(t) - k_{eff}N_{CB}(t) \quad \text{(Eq. S8)}$$

$$\frac{dN_{eff}(t)}{dt} = k_{eff}N_{CB}(t) \quad \text{(Eq. S9)}$$

Considering that $k_i = 1/\tau_i$ (i = ET_1, ET_2 and *eff*), and imposing boundary conditions we analytically solve from (Eq. S6) to (Eq. S9):

$$N_{LUMO_1}(t) = N_{LUMO_1,0}\exp\left(-\frac{t}{\tau_{ET_1}}\right) \quad \text{(Eq. S10)}$$

$$N_{LUMO_2}(t) = N_{LUMO_2,0}\exp\left(-\frac{t}{\tau_{ET_2}}\right) \quad \text{(Eq. S11)}$$

$$N_{CB}(t) = N_{LUMO_1,0}\frac{\tau_{eff}}{\tau_{ET_1}-\tau_{eff}}\left[\exp\left(-\frac{t}{\tau_{ET_1}}\right) - \exp\left(-\frac{t}{\tau_{eff}}\right)\right] + N_{LUMO_2,0}\frac{\tau_{eff}}{\tau_{ET_2}-\tau_{eff}}\left[\exp\left(-\frac{t}{\tau_{ET_2}}\right) - \exp\left(-\frac{t}{\tau_{eff}}\right)\right] \quad \text{(Eq. S12)}$$

$$N_{eff}(t) = N_{LUMO_1,0}\frac{\tau_{ET_1}\left(1-\exp\left(-\frac{t}{\tau_{ET_1}}\right)\right)-\tau_{eff}\left(1-\exp\left(-\frac{t}{\tau_{eff}}\right)\right)}{\tau_{ET_1}-\tau_{eff}} + N_{LUMO_2,0}\frac{\tau_{ET_2}\left(1-\exp\left(-\frac{t}{\tau_{ET_2}}\right)\right)-\tau_{eff}\left(1-\exp\left(-\frac{t}{\tau_{eff}}\right)\right)}{\tau_{ET_2}-\tau_{eff}} \quad \text{(Eq. S13)}$$

S9. Equations of two ET model for fitting FLUPS and TRTS data

To fit the experimental data from FLUPS and TRTS measurements, we have applied a convolution function between the solutions of the differential equations and the Instrument Response Function of each setup:

$$(f * g)(t) = \int f(t_0)g(t-t_0)\,\mathrm{d}t_0 \quad \text{(Eq. S14)}$$

1) For the FLUPS data: We need to consider Instrument Response Function (IRF) of the FLUPS setup,

$$IRF_{FLUPS}(t) = \exp\left(-\frac{t}{\tau_{IRF}^{FLUPS}/2\ln 2}\right)^2 \quad \text{(Eq. S15)}$$

where τ_{IRF}^{FLUPS} is the temporal width of IRF in FLUPS.

1.1) C343 in solution: the temporal trace of the FL is then described by the convolution:

$$N_{\mathrm{C343}}^{FLUPS}(t) = IRF_{FLUPS}(t) * N_{LUMO}(t) \quad \text{(Eq. S16)}$$

Whose explicit form is:

$$N_{\mathrm{C343}}^{FLUPS}(t) = \exp\left(-\frac{t}{\tau_{IRF}^{FLUPS}/2\ln 2}\right)^2 * \left[A_{artf}\exp\left(-\frac{t}{\tau_{artf}}\right) + N_{LUMO,0}\exp\left(-\frac{t}{\tau_{\mathrm{C343}}}\right)\right] \quad \text{(Eq. S17)}$$

where we made $t_0 \equiv t_{0,\mathrm{C343}}^{FLUPS}$, the time zero in FLUPS for the C343 in solution and τ_{C343} is given by (Eq. S3). Solving analytically (Eq. S17) by applying (Eq. S14), we obtain an expression for fitting FLUPS data of the C343 in solution:

$$N_{\mathrm{C343}}^{FLUPS}(t) = A_{artf}\frac{1}{2}\exp\left(-\frac{t-t_{0,\mathrm{C343}}^{FLUPS}}{\tau_{artf}}\right)\exp\left(\frac{1}{16\ln 2}\left(\frac{\tau_{IRF}^{FLUPS}}{\tau_{artf}}\right)^2\right)\left(\mathrm{erf}\left(2\sqrt{\ln 2}\,\frac{t-t_{0,\mathrm{C343-SnO_2}}^{FLUPS}}{\tau_{IRF}} - \frac{1}{4\sqrt{\ln 2}}\frac{\tau_{IRF}^{FLUPS}}{\tau_{artf}}\right) + 1\right) + N_{LUMO,0}\frac{1}{2}\exp\left(-\frac{t-t_{0,\mathrm{C343}}^{FLUPS}}{\tau_{\mathrm{C343}}}\right)\exp\left(\frac{1}{16\ln 2}\left(\frac{\tau_{IRF}^{FLUPS}}{\tau_{\mathrm{C343}}}\right)^2\right)\left(\mathrm{erf}\left(2\sqrt{\ln 2}\,\frac{t-t_{0,\mathrm{C343}}^{FLUPS}}{\tau_{IRF}} - \frac{1}{4\sqrt{\ln 2}}\frac{\tau_{IRF}^{FLUPS}}{\tau_{\mathrm{C343}}}\right) + 1\right) \quad \text{(Eq. S18)}$$

where erf(t) is the error function.

1.2) C343-SnO_2 interface: According to the model proposed in S4, for the interface we ascribe each component of the temporal trace from FL to a competition between an independent ET and FL channels, as shown in (Eq. S5). In first approximation the temporal trace of the FL from the C343-SnO_2 interface

are given by a sum of (Eq. S10) and (Eq. S11), where we substitute the lifetimes with the ones given by (Eq. S5). Then, we can describe the FL of the interface as:

$$N^{FLUPS}_{\mathrm{C343-SnO_2}}(t) = N_{LUMO_1,0}\exp\left(-\frac{t}{\tau_{\mathrm{C343-SnO_2},1}}\right) + N_{LUMO_2,0}\exp\left(-\frac{t}{\tau_{\mathrm{C343-SnO_2},2}}\right) \quad \text{(Eq. S19)}$$

Including the convolution with the IRF of the FLUPS setup:

$$N^{FLUPS}_{\mathrm{C343-SnO_2}}(t)' = IRF_{FLUPS}(t) * N^{FLUPS}_{C343-\mathrm{SnO_2}}(t) \quad \text{(Eq. S20)}$$

Solving analytically (Eq. S20) by applying (Eq. S14), where we made $t_0 \equiv t_{0,\text{C343-SnO}_2}{}^{FLUPS}$, time zero in FLUPS for C343-SnO_2, we obtain an expression for fitting FLUPS data of the C343-SnO_2 interface:

$$N^{FLUPS}_{\mathrm{C343-SnO_2}}(t)' =$$
$$N_{LUMO_1,0}\frac{1}{2}\exp\left(-\frac{t-t^{FLUPS}_{0,\mathrm{C343-SnO_2}}}{\tau_{\mathrm{C343-SnO_2},1}}\right)\exp\left(\frac{1}{16\ln 2}\left(\frac{\tau^{FLUPS}_{IRF}}{\tau_{\mathrm{C343-SnO_2},1}}\right)^2\right)\left(\mathrm{erf}\left(2\sqrt{\ln 2}\,\frac{t-t^{FLUPS}_{0,\mathrm{C343-SnO_2}}}{\tau_{IRF}} - \frac{1}{4\sqrt{\ln 2}}\frac{\tau^{FLUPS}_{IRF}}{\tau_{\mathrm{C343-SnO_2},1}}\right)+1\right) +$$
$$N_{LUMO_2,0}\frac{1}{2}\exp\left(-\frac{t-t^{FLUPS}_{0,\mathrm{C343-SnO_2}}}{\tau_{\mathrm{C343-SnO_2},2}}\right)\exp\left(\frac{1}{16\ln 2}\left(\frac{\tau^{FLUPS}_{IRF}}{\tau_{\mathrm{C343-SnO_2},2}}\right)^2\right)\left(\mathrm{erf}\left(2\sqrt{\ln 2}\,\frac{t-t^{FLUPS}_{0,\mathrm{C343-SnO_2}}}{\tau_{IRF}} - \frac{1}{4\sqrt{\ln 2}}\frac{\tau^{FLUPS}_{IRF}}{\tau_{\mathrm{C343-SnO_2},2}}\right)+1\right) \quad \text{(Eq. S21)}$$

2) <u>For the TRTS data</u>: We need to consider Instrument Response Function (IRF) of the TRTS setup:

$$IRF_{TRTS}(t) = \exp\left(-\frac{t}{\tau^{TRTS}_{IRF}/2\ln 2}\right)^2 \quad \text{(Eq. S22)}$$

Then, we fit the TRTS data of the interface with the convolution between the IRF of the TRTS setup and (Eq. S11):

$$N^{TRTS}_{CB}(t) = \exp\left(-\frac{t}{\tau^{TRTS}_{IRF}/2\ln 2}\right)^2 * \left[N_{LUMO_1,0}\frac{\tau_{eff}}{\tau_{ET_1}-\tau_{eff}}e^{-t/\tau_{ET_1}} + N_{LUMO_2,0}\frac{\tau_{eff}}{\tau_{ET_2}-\tau_{eff}}e^{-t/\tau_{ET_2}} - \left(N_{LUMO_1,0}\frac{\tau_{eff}}{\tau_{ET_1}-\tau_{eff}} + N_{LUMO_2,0}\frac{\tau_{eff}}{\tau_{ET_2}-\tau_{eff}}\right)e^{-t/\tau_{eff}}\right] \quad \text{(Eq. S23)}$$

Solving analytically (Eq. S23) by applying (Eq. S14), we obtain an expression for fitting TRTS data of the C343-SnO_2 interface:

$$N^{TRTS}_{\mathrm{C343-SnO_2}}(t) = N_{LUMO_1,0}\frac{\tau_{eff}}{\tau_{ET_1}-\tau_{eff}}\frac{1}{2}\exp\left(-\frac{t-t^{TRTS}_0}{\tau_{ET_1}}\right)\exp\left(\frac{1}{16\ln 2}\left(\frac{\tau^{TRTS}_{IRF}}{\tau_{ET_1}}\right)^2\right)\left(\mathrm{erf}\left(2\sqrt{\ln 2}\,\frac{t-t^{TRTS}_0}{\tau_{IRF}} - \frac{1}{4\sqrt{\ln 2}}\frac{\tau^{TRTS}_{IRF}}{\tau_{ET_1}}\right)+1\right) + N_{LUMO_2,0}\frac{\tau_{eff}}{\tau_{ET_2}-\tau_{eff}}\frac{1}{2}\exp\left(-\frac{t-t^{TRTS}_0}{\tau_{ET_2}}\right)\exp\left(\frac{1}{16\ln 2}\left(\frac{\tau^{TRTS}_{IRF}}{\tau_{ET_2}}\right)^2\right)\left(\mathrm{erf}\left(2\sqrt{\ln 2}\,\frac{t-t^{TRTS}_0}{\tau_{IRF}} - \frac{1}{4\sqrt{\ln 2}}\frac{\tau^{TRTS}_{IRF}}{\tau_{ET_2}}\right)+1\right) - \left(N_{LUMO_1,0}\frac{\tau_{eff}}{\tau_{ET_1}-\tau_{eff}} +$$

$$N_{LUMO_2,0}\frac{\tau_{eff}}{\tau_{ET_2}-\tau_{eff}}\Big)\frac{1}{2}\exp\left(-\frac{t-t_0^{TRTS}}{\tau_{eff}}\right)\exp\left(\frac{1}{16\ln 2}\left(\frac{\tau_{IRF}^{TRTS}}{\tau_{eff}}\right)^2\right)\left(\mathrm{erf}\left(2\sqrt{\ln 2}\,\frac{t-t_0^{TRTS}}{\tau_{IRF}}-\frac{1}{4\sqrt{\ln 2}}\frac{\tau_{IRF}^{TRTS}}{\tau_{eff}}\right)+1\right)$$

(Eq. S24)

S10. Relative amplitudes of lifetimes and ET lifetimes in FLUPS and TRTS

The relative amplitude values given in main text for FLUPS data of C343-SnO_2 have been calculated using the following equations.

$$A_{\tau_{\mathrm{c343-Sno_2},1}}=\left|\frac{A_{\tau_{\mathrm{c343-Sno_2},1}}}{A_{\tau_{\mathrm{c343-Sno_2},1}}+A_{\tau_{\mathrm{c343-Sno_2},2}}}\right| \quad \text{(Eq. S25)}$$

$$\Delta A_{\tau_{\mathrm{c343-Sno_2},1}}=\left[\frac{\left|A_{\tau_{\mathrm{c343-Sno_2},2}}\right|\Delta A_{\tau_{\mathrm{c343-Sno_2},1}}+\left|A_{\tau_{\mathrm{c343-Sno_2},1}}\right|\Delta A_{\tau_{\mathrm{c343-Sno_2},2}}}{\left(A_{\tau_{\mathrm{c343-Sno_2},1}}+A_{\tau_{\mathrm{c343-Sno_2},2}}\right)^2}\right] \quad \text{(Eq. S26)}$$

$$A_{\tau_{\mathrm{c343-Sno_2},2}}=\left|\frac{A_{\tau_{\mathrm{c343-Sno_2},2}}}{A_{\tau_{\mathrm{c343-Sno_2},1}}+A_{\tau_{\mathrm{c343-Sno_2},2}}}\right| \quad \text{(Eq. S27)}$$

$$\Delta A_{\tau_{\mathrm{c343-Sno_2},2}}=\left[\frac{\left|A_{\tau_{\mathrm{c343-Sno_2},2}}\right|\Delta A_{\tau_{\mathrm{c343-Sno_2},1}}+\left|A_{\tau_{\mathrm{c343-Sno_2},1}}\right|\Delta A_{\tau_{\mathrm{c343-Sno_2},2}}}{\left(A_{\tau_{\mathrm{c343-Sno_2},1}}+A_{\tau_{\mathrm{c343-Sno_2},2}}\right)^2}\right] \quad \text{(Eq. S28)}$$

The relative amplitude values given in main text for TRTS data in C343-SnO_2 have been calculated using the following equations.

$$A_{ET_1}=\left|\frac{A_{\tau_{ET_1}}}{A_{\tau_{ET_1}}+A_{\tau_{ET_2}}}\right| \quad \text{(Eq. S29)}$$

$$\Delta A_{ET_1}=\left[\frac{\left|A_{\tau_{ET_2}}\right|\cdot\Delta A_{\tau_{ET_1}}+\left|A_{\tau_{ET_1}}\right|\cdot\Delta A_{\tau_{ET_2}}}{\left(A_{\tau_{ET_1}}+A_{\tau_{ET_2}}\right)^2}\right] \quad \text{(Eq. S30)}$$

$$A_{ET_2}=\left|\frac{A_{\tau_{ET_2}}}{A_{\tau_{ET_1}}+A_{\tau_{ET_2}}}\right| \quad \text{(Eq. S31)}$$

$$\Delta A_{ET_2}=\left[\frac{\left|A_{\tau_{ET_2}}\right|\cdot\Delta A_{\tau_{ET_1}}+\left|A_{\tau_{ET_1}}\right|\cdot\Delta A_{\tau_{ET_2}}}{\left(A_{\tau_{ET_1}}+A_{\tau_{ET_2}}\right)^2}\right] \quad \text{(Eq. S32)}$$

Once we have obtained the lifetimes in the C343 in solution and in the C343-SnO_2 interface, the subtraction between the inverse of (Eq. S5) and (Eq. S3) gives the ET lifetimes:[12]

$$\frac{1}{\tau_{\mathrm{C343-SnO_2},i}}-\frac{1}{\tau_{\mathrm{C343}}}=\left(k_{ET,i}+k_{FL}\right)-k_{FL}=k_{ET,i}=\frac{1}{\tau_{ET,i}} \quad \text{(Eq. S33)}$$

This conventional protocol assumes that the functionalization of the SnO_2 by C343 molecules 1) does not modify the properties of the molecules in solution; 2) is not introducing additional comparable channels beyond ET, *i.e.* all the quenching of the FL is ascribed to this effect, so $k_{FL}^{\text{C343-SnO2}} \approx k_{FL}^{\text{C343}}$; and 3) non-radiative channels from the dye in solution are not modified when C343 sensitize the SnO_2. From (Eq. S33) we have calculated the ET lifetimes from FLUPS as:

$$\tau_{ET,i} = \frac{1}{\frac{1}{\tau_{\text{C343-SnO}_2}} - \frac{1}{\tau_{\text{C343}}}}; \qquad \Delta\tau_{ET_i} = \frac{\frac{\Delta\tau_{\text{C343-SnO}_2,i}}{\tau^2_{\text{C343-SnO}_2,i}} + \frac{\Delta\tau_{\text{C343}}}{\tau^2_{\text{C343}}}}{\left(\frac{1}{\tau_{\text{C343-SnO}_2,i}} - \frac{1}{\tau_{\text{C343}}}\right)^2} \qquad \text{(Eq. S34)}$$

The uncertainty to the ET lifetime value from (Eq. S34) is calculated by error propagation.

S11. Comparison of steady-state PL and FLUPS measurements

The absorption and emission peaks of C343 in 0.1mM EtOH solution (Figure S7a) are located at 2.77 (grey line) and at 2.54 eV (red line), respectively, in good agreement with previous reports.[13-16,20-21] Regarding the FL spectrum of C343 in solution and of the C343-SnO_2 interface (Figure S7b), the broadening in the film (Figure S7c) could be due to two different conformations of the C343 molecules in the SnO_2 surface.

Figure S7d shows the normalized FL intensity on C343-SnO_2 film in two different spots, as well as in a SnO_2 film, from steady-state measurements. The maximum emission peak for the first spot (dark blue line) is located at 2.56 eV, and the two shoulders are located at 2.15 eV and 2.00 eV. For the second spot (light blue line), the maximum peak is located at 2.15 eV, and the two shoulders are located at 1.97 eV and 1.80 eV on the left of main peak, and one shoulder at 2.56 eV on the right of main peak. These differences indicates that, although the emission peaks for both spots are located at the same energies, their relative amplitudes depend on the spot on the C343-SnO_2 interface we are exciting. In other words, the different relative amplitudes between both spots are due to surface inhomogeneities of the C343-SnO_2 interface.

Figure S7e shows the normalized FL of C343 in a 0.01mM EtOH solution measured through steady-state PL (red line) and FLUPS (black line). The observed shift of 0.08 eV in the FL peak between both measurements might be due to the different sensitivities between steady-state PL and FLUPS setups and/or to small changes in C343 concentration between both measurements.

Figure S7f shows the normalized FL of the C343-SnO_2 film obtained from steady-state PL in two spots (light and dark blue) and through FLUPS (light yellow), as well as for the SnO_2 film (orange line), described in the previous paragraph. The position of the fluorescence peaks between both techniques in the C343-SnO_2 film have changed in 0.06 eV. Furthermore, the FL measurements by steady-state PL show a secondary shoulder at 2.00 eV, and another two around 1.96 eV and 1.80 eV, both being undetected by FLUPS since the filters in this setup need to absorb laser light to avoid artifacts. The available bandwidth in FLUPS (2.09 eV), since it might affect the relative amplitudes of the ET processes, as discussed for the

second global fit (Figure 3), does not alter the relevant kinetic processes analyzed in our study. Finally, the different available spectral windows between FLUPS and steady-state PL, the latter being wider and with better spectral resolution (Figure S5f), might results in an apparent shift of the position of the FL peaks.

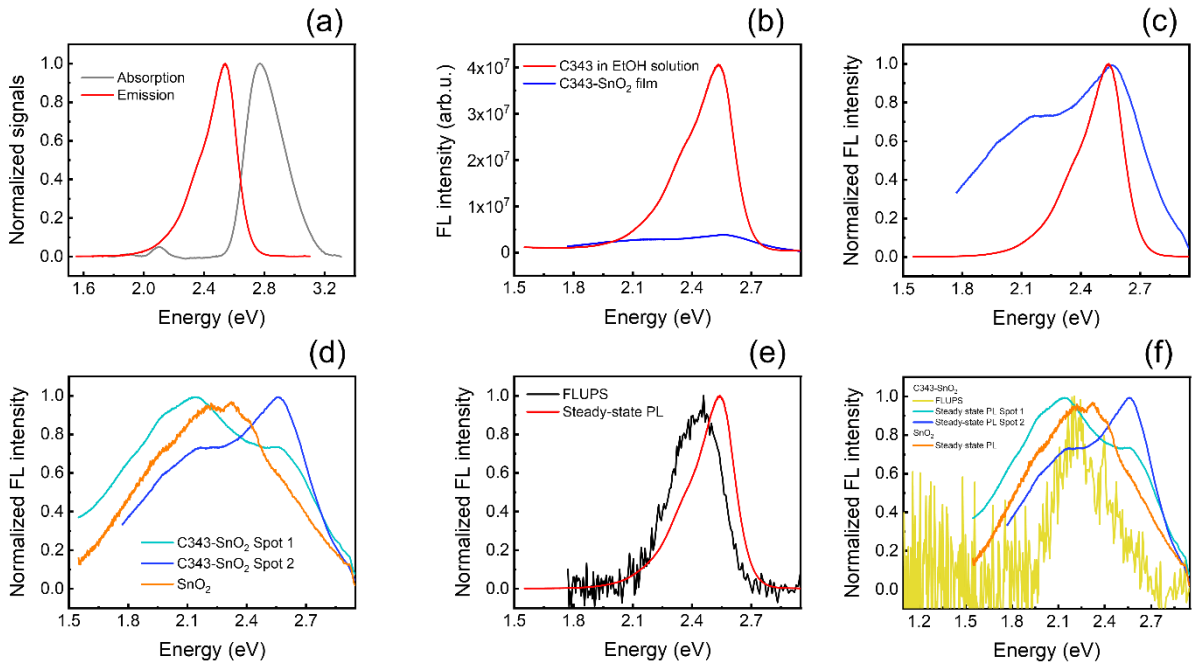

Figure S7. (a) Normalized absorption (grey line) and intensity of the FL (red line) for 0.01mM C343 in EtOH solution. We excite at 3.067 eV from pulsed laser with a repetition rate of 10MHz. Absorption peak is located at 2.77 eV, whereas the maximum emission peak is located at 2.54 eV. (b) Intensity of the FL intensity for C343 in 0.01mM EtOH solution (red line) and of C343-SnO_2 film (blue line), both measured by steady-state PL. (c) Normalized intensity of the FL of C343 in 0.01mM EtOH solution (red line) and of C343-SnO_2 film (blue line) measured through steady-state PL. We excite in (b) in the same condition that in (a). Maximum emission peak for the solution (red line) is located at 2.54 eV, whereas for the film is located at 2.56 eV with a shoulder at 2.15 eV. (d) Normalized steady-state PL measurements for the C343-SnO_2 film in two spots (light blue and dark blue) and on a SnO_2 film (orange). We excite in the same conditions that in (a). Maximum emission peak for the first spot (dark blue) is located at 2.56 eV, and the shoulder is located at 2.15 eV. For the second spot (light blue), maximum peak is located at 2.15 eV, and the shoulder on the right is at 2.56 eV. (e) Normalized intensity of the FL for C343 in a 0.01mM EtOH solution from FLUPS (black) and steady-state PL measurements (red). Peak intensity is located at 2.46 eV, whereas is located at 2.54 eV for steady-state measurements. (f) Normalized intensity of the FL for the C343-SnO_2 interface from FLUPS (light yellow line) and steady-state PL in different spots (light blue and dark blue), and from steady-state PL measurements on the SnO_2 alone (orange). For the C343 in solution, the maximum peaks in FLUPS are located at 2.21 eV and 2.50 eV, whereas peaks from steady-state PL measurements for both spots are located at 2.15 eV (light blue line) and 2.56 eV (dark blue line).

S12. TRTS measurements of SnO_2 film and C343 in solution

The employed pump energy in the TRTS experiment is smaller than the energy gap of the SnO_2, so we register no changes in the transmission of the SnO_2 (Figure S8, black dots). On the other hand, regarding the C343 in a EtOH solution, the photo generated carriers are bound molecular excitons, so there is no photo modulation of the THz amplitude, thus resulting as well in $-\Delta T = 0$ (Figure S8, red dots in the inset).

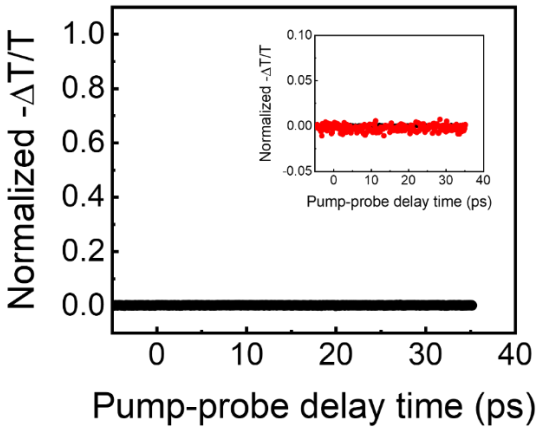

Figure S8. Optical pump-THz probe on pristine SnO_2. Inset: Zoom to compare with TRTS of the C343 in EtOH solution (red dots). Both samples have been measured at pump fluence of 1520 μJ/cm^2, and the temporal traces have been normalized by dividing the data set with the same maximum value used in the main text to normalize the temporal trace of the C343-SnO_2 film (see Figure 2a).

S13. Pump fluence dependence measurements in TRTS

We describe TRTS dynamics at (424 ± 15) μJ/cm^2 and (42 ± 2) μJ/cm^2 of a C343-SnO_2 film (Figure S9a) with two independent ETs pathways which come from independent C343 LUMO populations. Fitting TRTS data with the two independent ET model yields ETs lifetimes and their respective amplitudes that coincide within error (Table S2). When we measure another C343-SnO_2 film at three different pump fluences (Figure S9b), the signal to noise ratio does not allow us to obtain reliable ET lifetime values. We show TRTS differential transmission values measured in Film 1 (Figure S9a) and in Film 2 (Figure S9b). The linear behavior of differential transmission data from both films (Figure S9c, black and red fits lines) ensure first order carrier dynamics in the pump fluence that we have shown in main text.

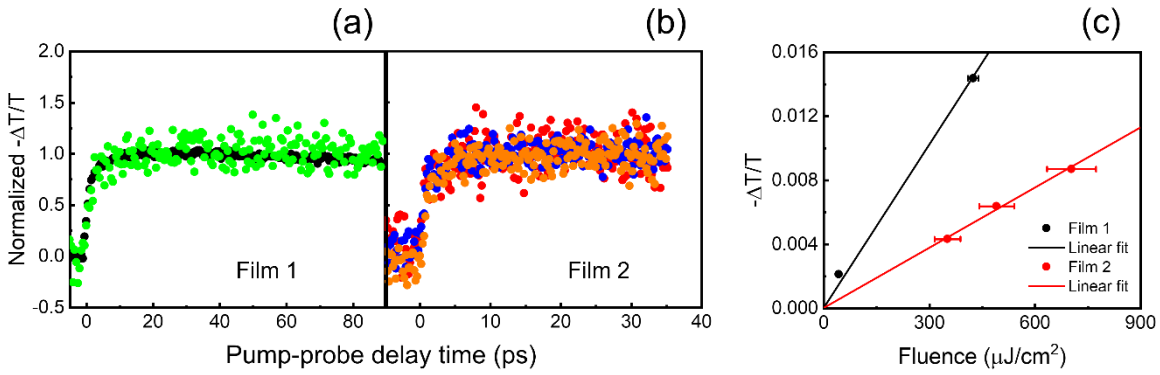

Figure S9. (a) TRTS normalized for two pump fluences (424 ± 15) μJ/cm^2, black dots; (42 ± 2) μJ/cm^2, green dots) for one C343-SnO_2 film (Film 1). (b) Same for another C343-SnO_2 film (Film 2) at three pump fluences: (350 ± 37) μJ/cm^2, red dots; (490 ± 50) μJ/cm^2, orange dots; (700 ± 70) μJ/cm^2, purple dots. (c) Normalized -ΔT/T, averaged between 20 and 40 ps, as a function of pump fluence for Film 1 (black solid dots) and Film 2 (black empty dots) and their linear fitting curve (black for Film 1, red for Film 2).

Fluence (μJ/cm^2)	$\tau_{ET,1}$ (ps)	Rel. Ampl. $\tau_{ET,1}$ (%)	$\tau_{ET,2}$ (ps)	Rel. Ampl. $\tau_{ET,2}$ (%)
42 ± 2	1.5 ± 0.6	70.5 ± 9.0	15.8 ± 6.4	29.5 ± 9.0
424 ± 15	1.4 ± 0.1	76.6 ± 2.8	9.7 ± 1.7	23.4 ± 2.8

Table S2. ETs lifetimes and their respective relative amplitudes (%) for two fluences in C343-SnO_2 TRTS measurements.

S14. Comparison of one and two electron transfer models fitting TRTS data

Despite a single-electron transfer fit does follow experimental data regarding faster electron transfer and back-electron transfer (Figure S10a), such fit is unable to reproduce data in the 2.5-25 ps time window, precisely the region where the slow electron transfer is expected to take place, as suggested with FLUPS measurements. Therefore, the residuals from the single-electron transfer model increase in that time window. On the contrary, the two-electron transfer fit can reproduce satisfactorily data in all the time window (Figure S10b), hence giving smaller residuals values than those from single-electron transfer fit, thus demonstrating the presence of two independent electron transfer processes.

(a) (b)

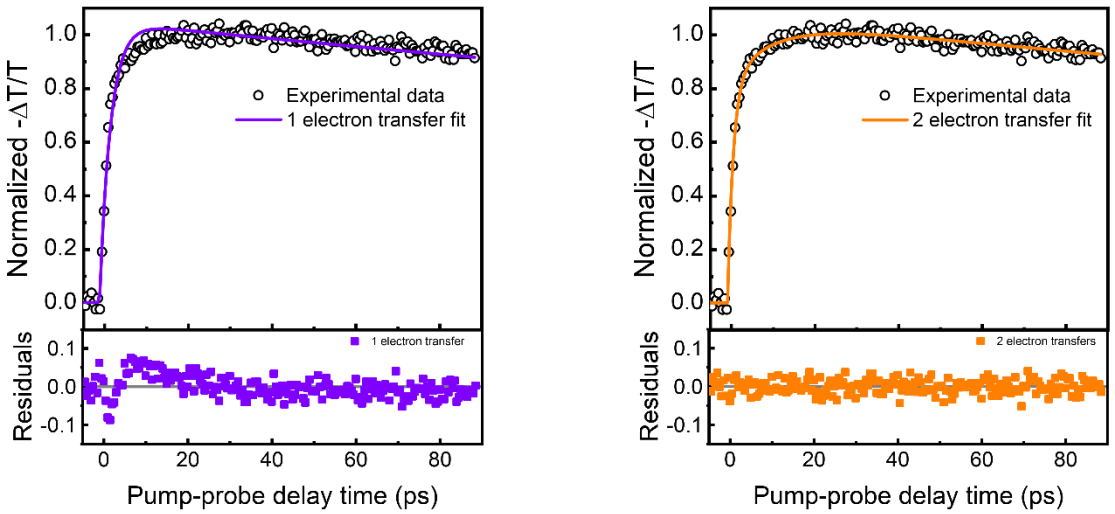

Figure S10. TRTS normalized data (black empty dots) are fitted with (a) single electron transfer model (purple line). Residuals from this fit curve are shown below; (b) two electron transfer model (orange line). Residuals from this fit are shown below.

S15. Drude-Smith model for frequency-resolved complex photoconductivity

We have used the Drude-Smith model to fit the photoconductivity of the C343-SnO_2 film:

$$\sigma_{DS}(\omega) = \frac{\varepsilon_0 \omega_p^2 \tau_s}{1-i\omega\tau}\left(1 + \frac{c}{1-i\omega\tau}\right) \quad \text{(Eq. S35)}$$

Where ε_0 is the vacuum permittivity, ω_p^2 is the plasmon frequency, τ_s the scattering time, and c the backscattering parameter. From fitting the frequency-resolved complex photoconductivity with (Eq. S35) we obtain ω_p^2, τ_s and c. The plasmon frequency ω_p^2 and the photocarrier density N are related through:

$$N = \frac{\varepsilon_0}{e^2} m^* \omega_p^2 \quad \text{(Eq. S36)}$$

In a Drude-Smith scenario, τ_s and μ are related through:

$$\mu = \frac{e\tau_s}{m^*}(1 + c) \quad \text{(Eq. S37)}$$

where m^*, ε_0 and e are the effective mass of the free electrons in the sample, the vacuum permittivity ($8.85 \cdot 10^{-12}$ F·m^{-1}) and the electric charge of electrons ($1.602 \cdot 10^{-19}$ C), respectively. From the Drude-Smith fit we have obtained that ω_p^2 = 11.5 ± 1.8 rad^2·ps^{-2}, τ_s = 0.20 ± 0.02 ps and c = -0.82 ± 0.01. The application of (Eq. S45) gives us that N = (1.5 ± 0.6)·10^{15} cm^{-3}. Since through TRTS we have monitored the electrons in the CB SnO_2, as m^* we have used the upper limit of the previously reported values, m^* = (0.41 ± 0.10)m_e,[22-23] where m_e is the electron mass ($9.109 \cdot 10^{-31}$ kg). Then, by applying (Eq. S37) we obtain a

conservative value of μ = (154 ± 60) $cm^2V^{-1}s^{-1}$. Under the assumption of a full absorption of the pump pulse by the film, the quantum yield is given by the ratio between the photocarrier density and the pump photon flux per unit volume, N_γ:

$$QY = \frac{N}{N_\gamma} \quad \text{(Eq. S38)}$$

where the N_γ can be obtained through:

$$N_\gamma = \frac{E_{pump}}{E_\gamma}\frac{1}{A \cdot l} \quad \text{(Eq. S39)}$$

Where E_{pump} is the pump pulse energy, E_γ is the pump beam photon energy, A the spot area of the pump pulse, and l the penetration depth of the pump photons in the C343-SnO_2 film. With the pump energy used to retrieve the photoconductivity of the C343-SnO_2 film, 4.75 μJ, the 400 nm photon energy, $4.97 \cdot 10^{-13}$ μJ, a pump diameter of 1.11 mm, and through the approximation of a homogeneous excitation profile of the pump pulse (l = 15 μm), by using (Eq. S39) we obtain N_γ = (6.6 ± 0.7)·10^{17} cm^{-3}. Finally, by applying (Eq. S38) we obtain a lower bound for the quantum yield of (2.3 ± 1.0)·10^{-3}.

S16. First global fit

To simultaneously fit both the temporal traces of FLUPS and TRTS we have used a Python script in a Jupyter notebook. First, we have combined the data from FLUPS and TRTS in common vectors for time and data. Then we have performed a simultaneous fit which imposes that the parameters of the ET lifetimes are shared for both temporal traces. Regarding the amplitudes, since the data from TRTS presents a rise, while the data from FLUPS shows an exponential decay, these parameters are not forced in the fit to be shared between both temporal traces, *i.e.* they remain as different parameters for each technique. The values of the amplitudes obtained from the first global fit (Table S3) are then used to calculate the relative amplitudes with their errors bars as shown above (see S10).

	Parameter	Fitted value
Shared lifetimes (ps)	τ_1	1.38 ± 0.06
	τ_2	17 ± 1
	τ_3	500 ± 100
FLUPS	A_1	7.0 ± 0.1
	A_2	2.63 ± 0.08
	A_3	0 ± 0.03
	t_0	0.101 ± 0.005
TRTS	A_1	-0.87 ± 0.03
	A_2	-0.25 ± 0.06
	t_0	-0.8 ± 0.1

Table S3. ET lifetimes and the amplitudes values obtained from the first global fit.

With $A_3^{TRTS} = -(A_1^{TRTS} + A_2^{TRTS})$.

S17. Second global fit

Using the temporal traces from FLUPS to retrieve the spectral fingerprint of the two ET lifetimes obtained with the first global fit, we have performed a second global fit with the built-in function of Igor Pro. To obtain the amplitudes we have forced the temporal traces from the FLUPS measurements on the C343-SnO_2 film for each probe energy between 2.03 and 2.70 eV to share the ET lifetimes obtained with the first global fit (see S16), leaving the amplitudes as free parameters. The results of the second global fit can be seen in Figure S11.

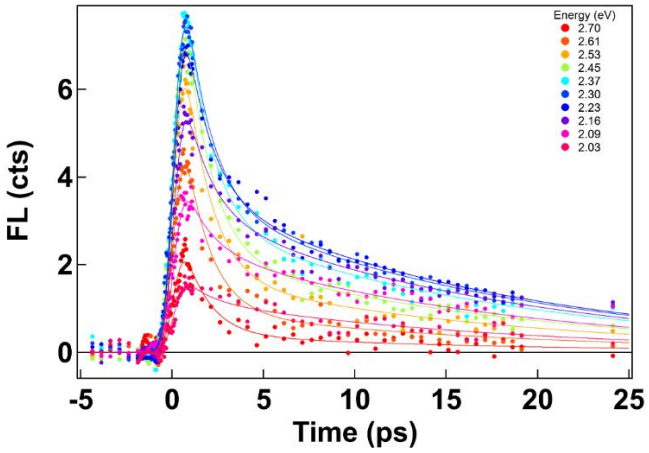

Figure S11. Temporal traces of the FL intensity at different energies fitted with the second global fit, which retrieve the spectral amplitudes of the ET lifetimes.

S18. Fitting TRTS data without considering convolution

Since IRF in TRTS is much lower than ET lifetimes, if we apply (Eq. S12) to fit TRTS data of C343-SnO_2 at a pump fluence of 424 μJ/cm^2 (Figure S12), we obtain ETs lifetimes and their respective amplitudes (Table S4) which are almost identical with those obtained by fitting the same TRTS data with (Eq. S24).

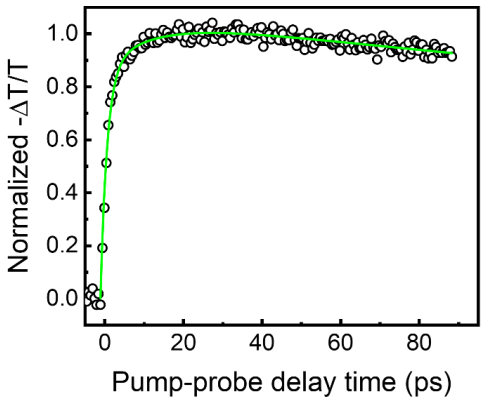

Figure S12. Normalized TRTS data (black squares dots) and fit curve applying (Eq. S35) for TRTS (solid green line) under a pump fluence of 424 μJ/cm^2.

TECHNIQUE	$\tau_{ET,1}$ **(ps)**	**Rel. Ampl.** $\tau_{ET,1}$ **(%)**	$\tau_{ET,2}$ **(ps)**	**Rel. Ampl.** $\tau_{ET,2}$ **(%)**
FLUPS (Eq. S21)	1.1 ± 0.1	79 ± 2	14 ± 2	21 ± 2
TRTS (Eq. S12)	1.7 ± 0.1	80 ± 3	12 ± 3	20 ± 3
TRTS (Eq. S24)	1.4 ± 0.1	77 ± 3	10 ± 2	23 ± 3

Table S4. Comparison of ETs lifetimes and their respective relative amplitudes from TRTS and FLUPS on a C343-SnO_2 film by applying (Eq. S21) for FLUPS data and (Eq. S12) and (Eq. S24) for TRTS data at a pump fluence of 424 μJ/cm^2.

▪ AUTHOR INFORMATION

Corresponding Author

Enrique Cánovas - *Instituto Madrileño de Estudios Avanzados en Nanociencia, calle Faraday 9, 28049 Madrid, Spain. E-mail*: enrique.canovas@imdea.org

Authors

Miguel Ángel Pulido Lendínez - *Instituto Madrileño de Estudios Avanzados en Nanociencia (IMDEA Nanociencia), Calle Faraday 9, 28049 Madrid, Spain.*

Marco Ballabio - *Instituto Madrileño de Estudios Avanzados en Nanociencia (IMDEA Nanociencia), Calle Faraday 9, 28049 Madrid, Spain.*

Andrés Burgos-Caminal - *Instituto Madrileño de Estudios Avanzados en Nanociencia (IMDEA Nanociencia), Calle Faraday 9, 28049 Madrid, Spain.*
Departamento de Química, Facultad de Ciencias, Universidad Autónoma de Madrid, Calle Francisco Tomás y Valiente 7, 28049 Madrid, Spain.

María E. Corrales - *Departamento de Química Física Aplicada, Facultad de Ciencias, Universidad Autónoma de Madrid, Calle Francisco Tomás y Valiente 8, 28049 Madrid, Spain.*
Departamento de Química, Facultad de Ciencias, Universidad Autónoma de Madrid, Calle Francisco Tomás y Valiente 7, 28049 Madrid, Spain.

Sergio Revuelta - *Instituto Madrileño de Estudios Avanzados en Nanociencia (IMDEA Nanociencia), Calle Faraday 9, 28049 Madrid, Spain.*

Saül Garcia-Orrit - *Instituto Madrileño de Estudios Avanzados en Nanociencia (IMDEA Nanociencia), Calle Faraday 9, 28049 Madrid, Spain.*

Víctor Vega-Mayoral - *Instituto Madrileño de Estudios Avanzados en Nanociencia (IMDEA Nanociencia), Calle Faraday 9, 28049 Madrid, Spain.*

Juan Cabanillas-González - *Instituto Madrileño de Estudios Avanzados en Nanociencia (IMDEA Nanociencia), Calle Faraday 9, 28049 Madrid, Spain.*

Luis Bañares - *Instituto Madrileño de Estudios Avanzados en Nanociencia (IMDEA Nanociencia), Calle Faraday 9, 28049 Madrid, Spain.*
Departamento de Química Física, Facultad de Ciencias Químicas, Universidad Complutense de Madrid, Plaza de las Ciencias, 2, 28040 Madrid, Spain.

Center for Ultrafast Lasers (CLUR), Facultad de Ciencias Químicas, Universidad Complutense de Madrid, Plaza de las Ciencias, 2, 28040 Madrid, Spain.

Wojciech Gawelda - *Instituto Madrileño de Estudios Avanzados en Nanociencia (IMDEA Nanociencia), Calle Faraday 9, 28049 Madrid, Spain.*

Departamento de Química, Facultad de Ciencias, Universidad Autónoma de Madrid, Calle Francisco Tomás y Valiente 7, 28049 Madrid, Spain.

Enrique Cánovas - *Instituto Madrileño de Estudios Avanzados en Nanociencia (IMDEA Nanociencia), Calle Faraday 9, 28049 Madrid, Spain.*

Notes

The authors declare no competing financial interests.

▪ REFERENCES

(1) H. Cheema, and J. H. Delcamp, "SnO_2 Transparent Printing Pastes from Powders for Photon Conversion in SnO_2 Based Dye-Sensitized Solar Cells", *Chem. Eur. J.* **2019**, 25(62), 14205-14213, https://doi.org/10.1002/chem.201903292

(2) J. Xu, Y. Wang, H. Shan, Y. Lin, Q. Chen, V. A. L. Roy, and Z. Xu, "Ultrasound-Induced Organogel Formation Followed by Thin Film Fabrication via Simple Doctor Blading Technique for Field-Effect Transistor Applications", *ACS Appl. Mater. Interfaces* 2016, 8, 29, 18991-18997, https://doi.org/10.1021/acsami.6b04817

(3) A. Berni, M. Mennig, and H. Schmidt, "Doctor Blade". In: Aegerter, M.A., Mennig, M. (eds) Sol-Gel Technologies for Glass Producers and Users. Springer, Boston, MA, 89-92 (2004), https://doi.org/10.1007/978-0-387-88953-5_10

(4) A. M. Jasim, A. S.J. Al-Zubaydi, and R. S. Zamel, "Influence of Heat Treatment on the Characteristic of SnO_2 Thin Films for Gas Sensor Application" (2021), *J. Phys.: Conf. Ser.* **1795** 012034, https://doi.org/10.1088/1742-6596/1795/1/012034

(5) J. M. Grey, J. M. Cole, and P. J. Evans, "Preferred Molecular Orientation of Coumarin 343 on TiO_2 Surfaces: Application to Dye-Sensitized Solar Cells", *ACS Appl. Mater. Interfaces* 2015, 7, 30, 16404-16409, https://doi.org/10.1021/acsami.5b03572

(6) R. S.-de-Armas, M. Á. San Miguel, J. Oviedo, and J. F. Sanz, "Coumarin derivatives for dye sensitized solar cells: a TD-DFT study", *Phys. Chem. Chem. Phys.* 2012, **14**, 225-233, https://doi.org/10.1039/C1CP22058F

(7) M. Grätzel, “Photoelectrochemical cells”, *Nature* **414**, 338-344 (2001), https://doi.org/10.1038/35104607

(8) R. Y. Korotkov, P. Ricou, A. J. E. Farran, “Preferred orientation in polycrystalline SnO_2 films grown by atmospheric pressure chemical vapor deposition”, *Thin Solid Films* 502 (2006), 79-87, https://doi.org/10.1016/j.tsf.2005.07.248

(9) M. Karmaoui, A. B. Jorge, P. F. McMillan, A. E. Aliev, R. C. Pullar, J. A. Labrincha, and D. M. Tobaldi, “One-Step Synthesis, Structure, and Band Gap Properties of SnO_2 Nanoparticles Made by a Low Temperature Nonaqueous Sol-Gel Technique”, *ACS Omega*, 2018, 3(10): 13227-1328, https://doi.org/10.1021/acsomega.8b02122. Corrected version in *ACS Omega*, 2018, 3, 16386-16386, https://doi.org/10.1021/acsomega.8b02860

(10) C. Sun, L. Bai, J. C. Roldao, A. Burgos-Caminal, O. Borrel-Grueiro, J. Lin, W. Huang, J. Gierschner, W. Gawelda, L. Bañares *et al*., “Boosting the Stimulated Emission Properties of Host:Guest Polymer Blends by Inserting Chain Twists in the Host Polymer”, *Adv. Funct. Mater.* **2022** 32(48), 2206723, https://doi.org/10.1002/adfm.202206723

(11) H. N. Ghosh, “Charge Transfer Emission in Coumarin 343 Sensitized TiO_2 Nanoparticle: A Direct Measurement of Back Electron Transfer”, *J. Phys. Chem. B* 1999, 103, 47, 10382-10387, https://doi.org/10.1021/jp9918611

(112) M. Ballabio, and E. Cánovas, “Electron Transfer at Quantum Dot-Metal Oxides Interfaces for Solar Energy Conversion”, *ACS Nanoscience Au* 2022, 2, 5, 367-395, https://doi.org/10.1021/acsnanoscienceau.2c00015

(13) L.-l. Jian, W.-l. Liu, Y.-f. Song, X. He, Y. Wang, H.-l. Wu, and Y.-q. Yang, “Solvent Effects on Spectral Property and Dipole Moment of the Lowest Excited State of Coumarin 343 Dye”, *Chin. J. Chem. Phys.* 25, 577 (2012), https://doi.org/10.1088/1674-0068/25/05/577-584

(14) K. Hara, T. Sato, R. Katoh, A. Furube, Y. Ohga, A. Shinpo, S. Suga, K. Sayama, H. Sugihara, and H. Arakawa, “Molecular Design of Coumarin Dyes for Efficient Dye-Sensitized Solar Cells”, *J. Phys. Chem. B* **2003**, 107, 2, 597-606, https://doi.org/10.1021/jp026963x

(15) H.-M. Tsai, J. S. Souris, H.-J. Kim, S.-H. Cheng, L. Chen, L.-W. Lo, C.-T. Chen, and C.-M. Kao, “Note: Rapid measurement of fluorescence lifetimes using SiPM detection and waveform sampling”, *Rev. Sci. Instrum.* **88**, 096107 (2017), https://doi.org/10.1063%2F1.5003413

(16) M. M. LaRocca, G. A. Baker, and M. P. Heitz, “Assesing rotation and solvation dynamics in ethaline deep eutectic solvent and its solution with methanol”, *J. Chem. Phys.* **155**, 034505 (2021), https://doi.org/10.1063/5.0056653

(17) J. R. Lakowicz, “Principles of Fluorescence Spectroscopy”, *Springer* (Third Edition, 2006)

(18) T. Kumpulainen, B. Lang, A. Rosspeintner, and E. Vauthey, “Ultrafast Elementary Photochemical Processes of Organic Molecules in Liquid Solution”, *Chem. Rev.* 2017, 117, 16, 10826-10939, https://doi.org/10.1021/acs.chemrev.6b00491

(19) A. Nazarov, A. I. Ivanov, A. Rosspeintner, and G. Angulo, “Full relaxation dynamics recovery from ultrafast fluorescence experiments by means of the stochastic model: Does the solvent response dynamics depend on the fluorophore nature?”, *Journal of Molecular Liquids* 360 (2022) 119387, https://doi.org/10.1016/j.molliq.2022.119387

(20) E. S. Savenko, and V. V. Kostjukov, “Coumarin 343 in aqueous solution: theoretical analysis of absorption”, *J. Mol. Model.* **28**, 126 (2022), https://doi.org/10.1007/s00894-022-05122-x

(21) D. Pant, and H. H. Girault, “Time-resolved total internal reflection fluorescence spectroscopy. Part I. Photophysics of Coumarin 343 at liquid/liquid interface, *Phys. Chem. Chem. Phys*., 2005, 7, 3457-3463, https://doi.org/10.1039/B507830J

(22) M. Nagasawa, S. Shionoya, and S. Makishima, “Electron Effective Mass of SnO_2”, *J. Phys. Soc. Jpn.* **20**, pp. 1093-1093 (1965), https://doi.org/10.1143/JPSJ.20.1093

(23) G. Sanon, R. Rup, and A. Mansingh, “Band-gap narrowing and band structure in degenerate tin oxide (SnO_2) films”, *Phys. Rev. B* **44**, 11, pp. 5672-5680, https://doi.org/10.1103/PhysRevB.44.5672